Source-Channel Communication Protocols and Tradeoffs in Active Wireless Sensing

Akbar M. Sayeed and Thiagarajan Sivanadyan
Department of Electrical and Computer Engineering
University of Wisconsin–Madison
akbar@engr.wisc.edu thiagars@cae.wisc.edu

***Abstract*— Active Wireless Sensing (AWS) is motivated by emerging advances in wireless technology and offers an alternative and complementary approach to in-network processing for rapid and energy-efficient information retrieval in wireless sensor networks. The basic architecture in AWS consists of: i) a wireless information retriever (WIR), equipped with an antenna array, that interrogates a select ensemble of wireless sensors with space-time waveforms, ii) the sensors acting as active scatterers – modulating the acquired waveforms with their (possibly encoded) measured data – to generate a multipath response to the WIR's interrogation signal, and iii) the WIR retrieving the sensor data by exploiting the space-time characteristics of the resulting multipath sensing channel. An important feature of AWS is its flexibility in tailoring the space-time interrogation waveforms, sensor encoding strategies, and associated processing of the received multipath signal at the WIR for energy-efficient information retrieval. A key mechanism for energy efficiency is distributed source-channel matching: generating a coherent response from sub-ensembles of sensors with highly correlated data, based on the spatial smoothness or correlation in the signal field or on the spatial scale of local cooperation in the network. In this paper, we will discuss a family of source-channel matching protocols in AWS and associated tradeoffs involving rate, reliability and energy consumption of information retrieval.**

I. Introduction

Existing approaches to information extraction in a wireless sensor network are heavily geared towards in-network processing where either the network as a whole obtains a consistent estimate of desired information (e.g., field data, or some summary statistic), or the distributed information is routed to a decision center via multi-hop routing (see, e.g., [1], [2]). However, in-network processing generally incurs excess delay and energy consumption due to the related tasks of information routing and coordination between nodes. In [3] we proposed an alternative approach – Active Wireless Sensing (AWS) – in which a wireless information retriever (WIR) interrogates a select ensemble of sensor nodes for rapid and energy-efficient retrieval of desired information (see Fig. 1). AWS has two primary attributes: i) the sensor nodes are relatively "dumb" in that they have limited computational power, and ii) the WIR is computationally powerful, is equipped with a multi-antenna array, and initiates the information retrieval by interrogating the nodes with wideband space-time waveforms. The basic concept of AWS is inspired by an intimate connection with communication over space-time multiple antenna (MIMO) wireless channels in a multipath environment: sensor nodes act as active scatterers and generate a multipath signal in response to WIR's interrogation signal. A key idea behind AWS is to separate multiple sensor responses by resolving the multipath signals in angle and delay at a resolution commensurate with the spatio-temporal signal space (see Figs. 1 and 2). This is facilitated by a virtual representation of wideband space-time wireless channels that we have developed in the past several years [4], [5]. In particular, the virtual representation yields a natural partitioning of sensor responses in angle-delay and provides a mathematical framework for studying fundamental limits of information retrieval in AWS at different spatio-temporal resolutions afforded by agile RF front-ends and reconfigurable antenna arrays [6]. Indeed, technological advances in agile RF front-ends provide another motivation for Active Wireless Sensing: WIR's equipped with agile RF transceivers could potentially enable rapid learning of sensor field structure at varying spatio-temporal resolutions. Such WIR's could also be integrated with strategically located access points for network state monitoring and control.

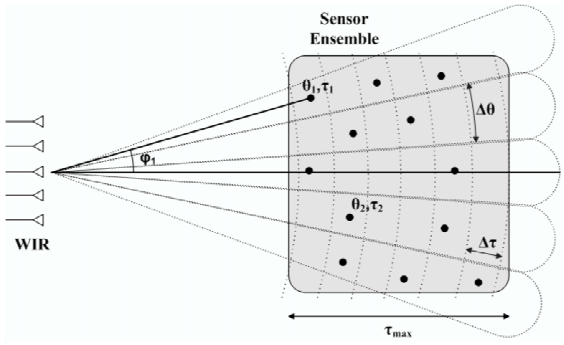

Fig. 1. Active Wireless Sensing: basic communication architecture.

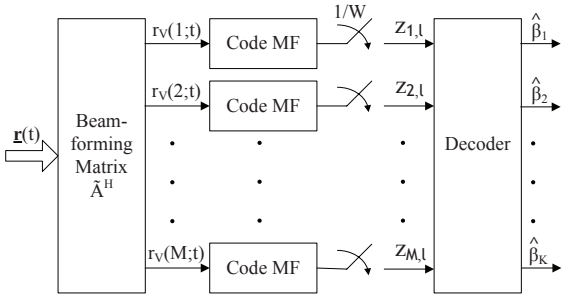

Fig. 2. Computation of sufficient statistics at the WIR.

An important feature of AWS is its flexibility in tailoring the space-time interrogation waveforms, sensor encoding strategies, and associated processing of the received multipath signal at the WIR for energy-efficient information retrieval. A key mechanism for energy efficiency is distributed source-channel matching: generating a coherent response from sub-ensembles of sensors with highly correlated data, based on the spatial smoothness or correlation in the signal field or on the spatial scale of local cooperation in the network. In this paper, we present a family of source-channel matching protocols in AWS and associated tradeoffs involving rate, reliability and energy consumption of information retrieval.

AWS is similar, in terms of the underlying physics, to the concept of Imaging Sensor Nets that has been independently proposed recently [7], [8]. However, the basic underlying methodology in these works, inspired by radar imaging principles, is quite different and focusses on sensor localization and detection of spatially well-separated events. Our emphasis, in contrast, is on high-rate sensor information retrieval and we exploit connections with recent developments in space-time wireless communications theory. We believe that these two related approaches provide complementary perspectives on information extraction in sensor networks and could be fruitfully cross-leveraged by exploring the connections between wideband radar imaging and wideband wireless communications in the context of sensor networks.

The next section reviews the basic space-time communication architecture in AWS and the computation of sufficient statistics at the WIR for sensor information retrieval. In Section III, we present a family of canonical sensing configurations representing different scales of correlation in the signal field. Section IV analyzes the performance of information retrieval at the highest spatio-temporal resolution. In Section V, we discuss information retrieval with distributed source-channel matching and quantify the associated gains in energy-efficiency. Section VI discusses the notion of sensing capacity in AWS. In all sections, we present numerical results to illustrate the theory.

II. The Basic Space-Time Communication Architecture

Consider an ensemble of K sensors uniformly distributed over a region of interest, as illustrated in Fig. 1. We first outline the basic assumptions made in this work. We assume that the WIR, equipped with an M-element array, is sufficiently far from the sensor ensemble, in the same plane, so that far-field assumptions apply. Furthermore, there exists a strong line of sight path between the WIR and each sensor (no fading) and the difference in path loss between individual sensors and the WIR can be neglected due to the large distance between the WIR and the sensor field. The WIR interrogates the sensor ensemble by transmitting wideband (spread-spectrum) signaling waveforms, $\{s_m(t)\}$, from different antennas where each $s_m(t)$ is of duration T and (two-sided) bandwidth W. Let $N = TW \gg 1$ denote the time-bandwidth product of the signaling waveforms that represents the approximate dimension of the temporal signal space. Thus, the signal space of spatio-temporal interrogation waveforms has dimension $MN = MTW$. Information retrieval at the highest angle-delay resolution, as elaborated later (see also [3]) constrain the bandwidth to: $c/\Delta d < W < 2f_c/M$ where f_c is the carrier frequency, c is the speed of wave propagation, and Δd is the minimum distance between the sensors. The above constraints also imply that $f_c > cM/2\Delta d$. For example, for a sensor separation of $\Delta d = 1$m, a WIR with $M = 10$ antennas uses a signaling bandwidth $W \geq 300$MHz, and a carrier frequency f_c on the order of a few GHz.

A. The Multipath Sensing Channel in AWS

We make the practically feasible assumption that the WIR and the sensor nodes are carrier (frequency) synchronized but not phase synchronized. Furthermore, we assume that the phase offset between each sensor and the WIR stays constant at least during two channel uses (each channel use corresponds to the signaling duration T). The basic communication protocol consists of the WIR transmitting the space-time signal $\boldsymbol{s}(t) = [s_1(t), s_1(t), \ldots, s_M(t)]^T$ in an interrogation packet to initiate information retrieval from the sensor ensemble. For simplicity, we consider a one-dimensional uniform linear array (ULA) and assume M to be odd WLOG, and define $\tilde{M} = (M-1)/2$. The array steering/response vector for a ULA is given by

$$\boldsymbol{a}(\theta) = \left[e^{j2\pi\tilde{M}\theta}, \ldots, 1, \ldots, e^{-j2\pi\tilde{M}\theta}\right]^T \quad (1)$$

where the normalized angle θ is related to the physical angle of arrival/departure φ (see Fig. 1) as $\theta = d\sin(\varphi)/\lambda$. Here d denotes the spacing between the antennas and λ is the wavelength of propagation. The steering/response vector represents the relative phases across antennas for transmitting/receiving a beam in the direction θ. We assume that the sensor ensemble projects a maximum angular spread (180 degrees) at the WIR array at $d = \lambda/2$ spacing; larger spacings can be used for smaller angular spreads.[1]

The i-th sensor acquires a waveform, $x_i(t)$, that is a superposition of the transmitted signal [3]

$$x_i(t) = e^{-j\phi_i}\boldsymbol{a}^T(\theta_i)\boldsymbol{s}(t-\tau_i) \quad (2)$$

where θ_i denotes the direction of the i-th sensor relative to the WIR array (see Fig. 1), τ_i denotes the relative delay between the i-th sensor and the WIR and ϕ_i denotes a random relative phase between the WIR and the i-th sensor. The i-th sensor encodes its measurement in β_i and modulates $x_i(t)$ by β_i and transmits it with energy $\mathcal{E}$ after a fixed duration (same for all sensors) following the reception of the interrogation packet. We assume instantaneous retransmission from each sensor for simplicity. Thus, the transmitted signal from the i-th sensor can be expressed as

$$y_i(t) = \beta_i\sqrt{\frac{\mathcal{E}}{M}}x_i(t) = \beta_i\sqrt{\frac{\mathcal{E}}{M}}e^{-j\phi_i}\boldsymbol{a}^T(\theta_i)\boldsymbol{s}(t-\tau_i) \quad (3)$$

[1] $d = \lambda/2\sin(\varphi_{max})$ spacing results is a one-to-one mapping between $\theta \in [-0.5, 0.5]$ and $\varphi \in [-\varphi_{max}, \varphi_{max}] \subset [-\pi/2, \pi/2]$.

where $E[|\beta_i|^2] = 1$ and $\int E[|x_i(t)|^2]dt = M$ so that $y_i(t)$ has energy $\mathcal{E}$. The received vector signal at the WIR, $\boldsymbol{r}(t) = [r_1(t), r_2(t), \cdots, r_M(t)]^T$, is a superposition of all sensor transmissions and by the principle of reciprocity it can be expressed as

$$\boldsymbol{r}(t) = \sqrt{\frac{\mathcal{E}}{M}} \sum_{i=1}^{K} \beta_i e^{-j\phi_i} \boldsymbol{a}(\theta_i)\boldsymbol{a}^T(\theta_i)\boldsymbol{s}(t-\tilde{\tau}_i) + \boldsymbol{w}(t) \quad (4)$$

where $\tilde{\tau}_i = 2\tau_i$ denotes the round-trip relative delay in the response from the i^{th} sensor, $\boldsymbol{w}(t)$ denotes an AWGN vector process representing the noise at different WIR antennas. Let $\tau_{max} = \max_i \tau_i$ and assume that $\min_i \tau_i = 0$ WLOG. Using (4), the effective system equation relating the received vector signal at the WIR to the transmitted interrogation signal can be expressed as

$$\boldsymbol{r}(t) = \sqrt{\frac{\mathcal{E}}{M}} \int_0^{2\tau_{max}} \boldsymbol{H}(t')\boldsymbol{s}(t-t')dt' + \boldsymbol{w}(t) \quad (5)$$

$$\boldsymbol{H}(t) = \sum_{i=1}^{K} \alpha_i \delta(t-\tilde{\tau}_i)\boldsymbol{a}(\theta_i)\boldsymbol{a}^T(\theta_i) \quad (6)$$

where $\alpha_i = \beta_i e^{-j\phi_i}$, and the $M \times M$ matrix $\boldsymbol{H}(t)$ represents the impulse response for the space-time multipath channel underlying AWS. The delay spread of the channel is $2\tau_{max}$ and we assume that the signaling duration $T \gg 2\tau_{max}$.

Note that the system representation (5), even though it relates the transmitted interrogation signal $\boldsymbol{s}(t)$ to the received signal at the WIR, is independent of the power used for transmitting the interrogation packet. This is because after acquiring the signaling waveform in the interrogation phase, each sensor retransmits it with energy $\mathcal{E}$ and the factor $\sqrt{\mathcal{E}}/\sqrt{M}$ reflects this normalization. Each transmission from the sensor ensemble of duration T defines a single channel use for information retrieval.

B. Sensor Localization Via Multipath Resolution

The active sensing channel matrix (6) has exactly the same form as the impulse response of a physical multiple-antenna (MIMO) multipath wireless channel where the sensor data and phases $\{\alpha_i = \beta_i e^{-j\phi_i}\}$ in the sensing channel correspond to the complex path gains associated with scattering paths in a MIMO multipath channel [4], [5]. We leverage the *virtual representation* of MIMO multipath channels that is a *unitarily equivalent* representation of the physical sensing channel matrix [4], [5]. A key property of the virtual channel representation is that its coefficients represent a resolution of sensors in angle and delay (and Doppler in case of relative motion, not considered in this paper) commensurate with the signal space parameters M and W (and T), respectively.

The virtual representation in angle corresponds to beamforming in M fixed virtual directions: $\tilde{\theta}_m = m/M$, $m = -\tilde{M}, \cdots, \tilde{M}$. Define the $M \times M$ unitary (DFT) matrix

$$\boldsymbol{A} = \frac{1}{\sqrt{M}}[\boldsymbol{a}(-\tilde{M}/M), \ldots, 1, \ldots, \boldsymbol{a}(\tilde{M}/M)] \quad (7)$$

whose columns are the normalized steering vectors for the virtual angles and form an orthonormal basis for the spatial signal space. The virtual spatial matrix $\boldsymbol{H}_V(t)$ is unitarily equivalent to $\boldsymbol{H}(t)$ as

$$\boldsymbol{H}(t) = \boldsymbol{A}\boldsymbol{H}_V(t)\boldsymbol{A}^T \leftrightarrow \boldsymbol{H}_V(t) = \boldsymbol{A}^H\boldsymbol{H}(t)\boldsymbol{A}^* \quad (8)$$

and the virtual coefficients, representing the coupling between the m-th transmit beam and m'-th receive beam are given by

$$H_V(m', m; t) = \boldsymbol{a}^H(m'/M)\boldsymbol{H}(t)\boldsymbol{a}^*(m/M)/M \quad (9)$$

$$= M \sum_{i=1}^{K} \alpha_i g\left(\theta_i - \frac{m'}{M}\right) g\left(\theta_i - \frac{m}{M}\right) \delta(t-\tilde{\tau}_i) \quad (10)$$

$$\approx \quad H_V(m, m; t)\delta_{m-m'} \quad (11)$$

$$H_V(m, m; t) \approx M \sum_{i \in S_{\theta,m}} \alpha_i g^2\left(\theta_i - \frac{m}{M}\right) \delta(t-\tilde{\tau}_i) \quad (12)$$

where $g(\theta) = \frac{1}{M}\frac{\sin(\pi M\ \theta)}{\sin(\pi\theta)}$ is the Dirichlet sinc function that captures the interaction between the fixed virtual beams and true sensor directions, δ_m denotes the kronecker delta function, and the last approximation follows from the virtual path partitioning [4]: $S_{\theta,m} = \{i \in \{1, \cdots, K\} : -1/2M < \theta_i - m/M \leq 1/2M\}$ denotes the set of all sensors whose angles lie in the m-th spatial resolution bin of width $\Delta\theta = 1/M$, centered around the m-th beam. Thus, the virtual spatial representation partitions the sensors in angle: it is approximately diagonal and its m-th diagonal entry contains the superposition of all sensor responses that lie within the m-th beam of width $1/M$.

The sensor responses within each spatial beam can be further partitioned by resolving their delays with resolution $\Delta\tau = 1/W$. Let $L = \lceil 2\tau_{max}W \rceil$ be the largest normalized relative delay. The diagonal entries of virtual spatial matrix can be further decomposed into virtual, uniformly spaced delays as [5]

$$H_V(m, m; t) \approx \sum_{\ell=0}^{L} H_V(m, m, \ell)\delta(t - \ell/W) \quad (13)$$

$$H_V(m, m, \ell) = M \sum_{i=1}^{K} \alpha_i g^2\left(\theta_i - \frac{m}{M}\right) \mathrm{sinc}(W\tilde{\tau}_i - \ell) \quad (14)$$

$$\approx M \sum_{i \in S_{\theta,m} \cap S_{\tau,\ell}} \alpha_i g^2\left(\theta_i - \frac{m}{M}\right) \mathrm{sinc}(W\tilde{\tau}_i - \ell) \quad (15)$$

where $\mathrm{sinc}(x) = \sin(\pi x)/\pi x$ captures the interaction between the fixed virtual and true sensor delays, and $S_{\tau,\ell} = \{i : -1/2W < \tilde{\tau}_i - \ell/W \leq 1/2W\}$ is the set of all sensors whose relative delays lie within the ℓ-th delay resolution bin of width $\Delta\tau = 1/W$.

Thus, the angle-delay virtual representation partitions the sensor responses into distinct angle-delay resolution bins: the virtual coefficient $H_V(m, m, \ell)$ is a superposition of all sensor responses whose angles and delays lie in the intersection of m-th spatial beam and ℓ-th delay ring (see Fig. 1). For a given number of antennas M and a given minimum spacing between sensors Δd, the bandwidth W can be chosen sufficiently large ($W > c/\Delta d$), in principle, so

that there is exactly one sensor in each angle-delay resolution bin. In this highest-resolution case, we can define one-to-one mappings $i(m,\ell)$ and $(m(i),\ell(i))$ that associate each sensor with a unique angle-delay resolution bin. It follows from (15) that information retrieval from the i-th sensor amounts to estimating the corresponding virtual angle-delay coefficient

$$\begin{aligned} h_V(m,\ell) &= H_V(m,m,\ell) \leftrightarrow M\beta_{i(m,\ell)}\gamma_{i(m,\ell)} \quad (16)\\ \gamma_{i(m,\ell)} &= e^{-j\phi_i} g^2(\theta_i - m/M)\mathrm{sinc}(W\tilde{\tau}_i - \ell)|_{i=i(m,\ell)} \ . \end{aligned}$$

We note that above development emphasizes the virtual coefficient that primarily carries information form the i-sensor resolved in the $(m(i),\ell(i))$-th angle-delay resolution bin. In general, there will be interference between the sensor responses, as elaborated next.

C. Angle-Delay Sufficient Statistics

We now describe the basic processing of the received signal $\boldsymbol{r}(t)$ at the WIR for computing the sufficient statistics for information retrieval, as illustrated in Fig. 2. Define $\boldsymbol{s}(t) = \boldsymbol{A}^* \boldsymbol{s}_V(t)$ and $\boldsymbol{r}_V(t) = \boldsymbol{A}^H \boldsymbol{r}(t)$ where $\boldsymbol{s}_V(t)$ and $\boldsymbol{r}_V(t)$ are the M-dimensional transmitted and received signals in the virtual spatial domain (beamspace). In our model, $\boldsymbol{s}_V(t)$ represents the temporal codes acquired by the sensors in different virtual spatial bins. Using (5), (8) and (13), the system equation (ignoring the fixed delay in re-transmission by the sensor nodes) that relates the received signal to the transmitted signal in the beamspace is

$$\boldsymbol{r}_V(t) = \sqrt{\frac{\mathcal{E}}{M}} \sum_{\ell=0}^{L} \boldsymbol{H}_V(\ell)\boldsymbol{s}_V(t-\ell/W) + \boldsymbol{w}_V(t) \quad (17)$$

where $\boldsymbol{H}_V(\ell)$ represents the virtual spatial matrix corresponding to the ℓ-th virtual delay and $\boldsymbol{w}_V(t)$ represents a vector of independent temporal white AWGN processes with PSD σ^2. Each $\boldsymbol{s}_V(m;t)$, the m-th component of $\boldsymbol{s}_V(t)$, is a unit-energy pseudo-random waveform with bandwidth W and duration T (e.g., a direct-sequence spread spectrum waveform), and we have[2]

$$\langle \boldsymbol{s}_V(m;t-\ell/W), \boldsymbol{s}_V(m;t-\ell'/W)\rangle \approx \delta_{\ell-\ell'} \ . \quad (18)$$

Thus, correlating each $\boldsymbol{r}_V(m;t)$ with delay versions of $\boldsymbol{s}_V(m;t)$ yields the sufficient statistics for information retrieval $\{z_{m,\ell} : m = -\tilde{M},\cdots,\tilde{M}; \ell = 0,\cdots,L\}$:

$$\begin{aligned} z_{m,\ell} &= \langle \boldsymbol{r}_V(m;t), \boldsymbol{s}_V(m;t-\ell/W)\rangle \quad (19)\\ &= \int_0^{T+2\tau_{max}} \boldsymbol{r}_V(m,t)\boldsymbol{s}_V^*(m,t-\ell/W)dt \ . \quad (20) \end{aligned}$$

Remark 1 (Ideal Case): In general, the matched-filter outputs in (20) include the desired response from the sensor in the (m,ℓ)-th angle-delay resolution bin as well as interference from sensors in other resolution bins. Such interference is virtually eliminated in the ideal situation when the sensors positions coincide with the center of the resolution bins; that is, $(\theta_i,\tau_i) = (m/M,\ell/W)$ for some $m \in \{-\tilde{M},\ldots,\tilde{M}\}$ and $\ell \in \{0,\ldots,L-1\}$. In this case, $z_{m,\ell}$ simplifies to

$$z_{m,\ell} = \sqrt{M\mathcal{E}}\beta_{i(m,\ell)}\gamma_{i(m,\ell)} + w_{m,\ell} \ , \quad (21)$$

where $\{w_{m,\ell}\}$ are i.i.d. Gaussian with variance σ^2. Note that the factor $\sqrt{M}$ reflects the M-fold array gain or the beamforming gain. □

While different temporal waveforms can be assigned to different spatial beams in AWS, in the rest of the paper we focus on the attractive special case in which the same spread-spectrum waveform, $c(t)$ is transmitted on all spatial beams; that is, $s_V(m;t) = c(t)$ for all m. We begin by assuming sufficient angle-delay resolution so that each sensor lies in a unique angle-delay resolution bin. We refer to the $K \le ML$ angle-delay resolution bins occupied by transmitting sensors to be "active". All further analysis and results presented in this paper assume that all the angle-delay bins are active i.e. $K = ML$. The matched filter outputs corresponding to the i-th active sensor can then be uniquely labeled by the mapping $z_{(m(i),\ell(i))} \mapsto z_i$ for $i = 1,..,K$. We can now express the matched filter outputs for active bins/sensors as

$$z_i = \sqrt{M\mathcal{E}}\beta_i\tilde{\gamma}_i + \sqrt{M\mathcal{E}}\sum_{k\neq i}\beta_k\tilde{\gamma}_{i,k} + w_i \quad (22)$$

where $\sqrt{M\mathcal{E}}\beta_i\tilde{\gamma}_i$ represents the desired signal component from the i-th sensor and $\beta_k\tilde{\gamma}_{i,k}$, $k \neq i$, represents the interference due to the other $K-1$ active sensors (in other distinct bins) where

$$\tilde{\gamma}_{i,k} = e^{-j\phi_k} g(\theta_k - m(i)/M)\mathrm{sinc}(W\tilde{\tau}_k - \ell(i)) \quad (23)$$

and $\tilde{\gamma}_i = \tilde{\gamma}_{i,i}$. The matched filter outputs $\{z_i = z_{m(i),\ell(i)} : i = 1,\cdots,K\}$ represent the sufficient statistics for information retrieval at the WIR. Note that when the sensors are ideally placed at the center of the angle-delay bins, $\tilde{\gamma}_{i,k} = 0$ for all $k \neq i$ and $|\tilde{\gamma}_i| = 1$ i.e. each MF output contains only the corresponding sensor's data with no interference (see (21)).

Stacking the MF outputs in a $K = ML$ dimensional vector, we have

$$\begin{aligned} \boldsymbol{z} &= \sqrt{M\mathcal{E}}\boldsymbol{\Gamma}\boldsymbol{\beta} + \boldsymbol{w} = \sqrt{M\mathcal{E}}\sum_{i=1}^{K}\beta_i\boldsymbol{\Gamma}_i + \boldsymbol{w} \quad (24)\\ \boldsymbol{\Gamma} &= [\boldsymbol{\Gamma}_2,\boldsymbol{\Gamma}_2,\cdots,\boldsymbol{\Gamma}_K] = [\tilde{\gamma}_{i,j}] \quad (25) \end{aligned}$$

where $\boldsymbol{\Gamma}$ is the $K\times K$ coupling matrix that maps the sensor data vector, $\boldsymbol{\beta} = [\beta_1 \ldots \beta_K]^T$, to the angle-delay MF output vector $\boldsymbol{z}$ and $\boldsymbol{w}$ is a complex AWGN vector with variance σ^2. The column vector $\boldsymbol{\Gamma}_k$ represents the *angle-delay signature* generated by the k-th sensor at the WIR.

III. Canonical Sensing Configurations

We now present a family of canonical sensing configurations in AWS that form the basis of this paper. For simplicity, we consider coherent BPSK transmissions from sensors: $\{\beta_i \in \{-1,+1\}\}$, and the phases $\{\phi_i\}$ are assumed known at the WIR. Phase estimation is possible if the phases $\{\phi_i\}$ are stable for at least two channel uses [3]. In this

[2]The cross-correlation is on the order of $1/N = 1/TW$ and thus very small for large N.

case, each sensor data transmission consists of two packets: a training packet of '$+1$' for phase estimation at the WIR followed by an information packet containing the information bit. We note that non-coherent (on-off) signaling can also be employed in AWS [3].

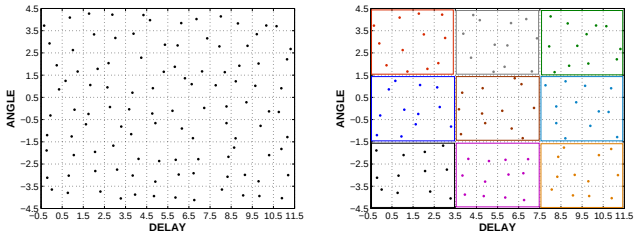

(a) (b)

Fig. 3. Illustration of canonical sensing configurations at maximum angle-delay resolution for $K = ML = 9 \times 12 = 108$ active sensors. The active sensors are partitioned as $K = K_{ind}K_{coh}$. (a) Independent transmissions from all sensors ($K_{ind} = 108$) (b) $K_{ind} = 9$ independent sensor transmissions with $K_{coh} = 12$ sensors transmitting each independent bit.

In the canonical sensing configurations, the $K = ML$ active sensors are partitioned into K_{ind} groups or *spatial coherence regions (SCR's)*, each group consisting of K_{coh} sensors so that $K = K_{ind}K_{coh}$, as illustrated in Fig. 3. We assume that all the K_{coh} sensors in each group transmit the same bit, whereas the bits from distinct groups are independent. That is, $\beta_i = \tilde{\beta}_\mu$ for all $i \in S_\mu$ where S_μ is the μ^{th} group of sensors in the μ^{th} SCR and the different $\tilde{\beta}_\mu$, $\mu = 1, \cdots, K_{ind}$ are independent. Thus, for a given value of K_{ind}, K_{ind} bits of information are retrieved in each channel use, whereas K_{coh} identical sensor measurements from each SCR increase energy-efficiency. The above sensing configurations are an idealized abstraction of correlated sensor measurements: all sensors within each group/SCR have highly correlated measurements, whereas the sensor measurements in different regions are statistically independent, corresponding to independent sensor measurements.

With the above partition of sensors, the K-dimensional sensor data vector $\boldsymbol{\beta}$ in (24) can be expressed as

$$\begin{aligned} \boldsymbol{\beta} &= \begin{bmatrix} \beta_1 \\ \beta_2 \\ \vdots \\ \beta_K \end{bmatrix} = \boldsymbol{U}\tilde{\boldsymbol{\beta}} \qquad (26) \\ &= \begin{bmatrix} \mathbf{1}_{K_{coh}} & \mathbf{0} & \cdots & \mathbf{0} \\ \mathbf{0} & \mathbf{1}_{K_{coh}} & \cdots & \mathbf{0} \\ \vdots & \vdots & \ddots & \mathbf{0} \\ \mathbf{0} & \mathbf{0} & \cdots & \mathbf{1}_{K_{coh}} \end{bmatrix} \begin{bmatrix} \tilde{\beta}_1 \\ \tilde{\beta}_2 \\ \vdots \\ \tilde{\beta}_{K_{ind}} \end{bmatrix} \end{aligned}$$

where $\mathbf{1}_{K_{coh}}$ is a column vector of size K_{coh} containing all '1's representing the correlated transmissions from the different sensors in a coherence group. The matrix $\boldsymbol{U}$ is a $K \times K_{ind}$ matrix that maps the K_{ind}-dimensional vector, $\tilde{\boldsymbol{\beta}}$, of independent information bits to the K-dimensional, $\boldsymbol{\beta}$, of sensor transmissions.

IV. Information Retrieval at Highest Resolution

In this section, we describe the signal processing at the WIR for information retrieval in the canonical sensing configurations in Section III at the highest angle-delay resolution: each angle-delay resolution bin corresponds to a distinct sensor. We analyze the resulting probability of error (P_e) in retrieving the K_{ind} bits of information in each channel use. Since we have K_{ind} independent data streams each consisting of K_{coh} copies, we assume WLOG that the first K_{coh} MF outputs correspond to the first sensor group, S_1, the second K_{coh} to group S_2 and so on. Then, the vector of MF outputs can be expressed as

$$\begin{aligned} \boldsymbol{z} &= [\boldsymbol{z}_1^T, \boldsymbol{z}_2^T, \cdots, \boldsymbol{z}_{K_{ind}}^T]^T \\ &= \sqrt{M\mathcal{E}}\boldsymbol{\Gamma}\boldsymbol{U}\tilde{\boldsymbol{\beta}} + \boldsymbol{w} = \sqrt{M\mathcal{E}}\boldsymbol{Q}\tilde{\boldsymbol{\beta}} + \boldsymbol{w} \\ &= \sqrt{M\mathcal{E}} \sum_{i=1}^{K_{ind}} \tilde{\beta}_i \boldsymbol{q}_i + \boldsymbol{w} \qquad (27) \end{aligned}$$

where each $\boldsymbol{z}_i$ is a $K_{coh} \times 1$ vector corresponding to the sensors in the i-th group and

$$\begin{aligned} \boldsymbol{Q} &= \boldsymbol{\Gamma}\boldsymbol{U} = [\boldsymbol{q}_1, \boldsymbol{q}_2, \cdots, \boldsymbol{q}_{K_{ind}}] \qquad (28) \\ \boldsymbol{q}_i &= \sum_{k \in S_i} \boldsymbol{\Gamma}_k \ , \ i = 1, \cdots, K_{ind} \ , \qquad (29) \end{aligned}$$

with $\boldsymbol{Q}$ being the $K \times K_{ind}$ matrix of *effective angle-delay signatures* that maps the K_{ind} independent bit streams in $\tilde{\boldsymbol{\beta}}$ to the K MF outputs $\boldsymbol{z}$, and $\boldsymbol{\Gamma}_k$ being the k^{th} column of $\boldsymbol{\Gamma}$ in (25).

A. Angle-Delay Signature Matched Filtering

Due to interference between angle-delay signatures of different sensors in (27), it is well-known that the optimal ML detector of the independent bit vector $\tilde{\boldsymbol{\beta}}$ has exponential complexity in K [9]. The simplest receiver structure simply ignores the interference and match filters to the angle-delay signatures of different sensors: $\hat{\tilde{\boldsymbol{\beta}}} = \text{sign}\{\text{Re}(\boldsymbol{Q}^H\boldsymbol{z})\}$. The i-th component of the decision statistics, $\tilde{\boldsymbol{z}} = \boldsymbol{Q}^H\boldsymbol{z}$, can be expressed as

$$\tilde{z}_i = \underbrace{\sqrt{M\mathcal{E}}(\boldsymbol{q}_i{}^H\boldsymbol{q}_i)\tilde{\beta}_i}_{S_i} + \underbrace{\sqrt{M\mathcal{E}}\sum_{k\neq i}(\boldsymbol{q}_i{}^H\boldsymbol{q}_k)\tilde{\beta}_k}_{I_i} + \underbrace{\boldsymbol{q}_i{}^H\boldsymbol{w}}_{N_i} \qquad (30)$$

where S_i represents the desired signal from the i-th coherence region, I_i the interference term, and N_i the noise. Using the Gaussian approximation for the interference I_i, the probability of error for the i-th bit stream can be characterized as [9]

$$P_e(i) = Q\left(\sqrt{2\text{SINR}(i)}\right) \qquad (31)$$

where the Signal-to-Interference-and-Noise-Ratio (SINR) is given by

$$\begin{aligned} \text{SINR}(i) &= \frac{E[|S_i|^2]}{E[|I_i|^2] + E[|N_i|^2]} \qquad (32) \\ &= \frac{2M\mathcal{E}\|\boldsymbol{q}_i\|^4}{\|\boldsymbol{q}_i\|^2\sigma^2 + M\mathcal{E}\sum_{k\neq i}|\boldsymbol{q}_i^H\boldsymbol{q}_k|^2} \qquad (33) \end{aligned}$$

Note that under ideal conditions, ${\mathbf{\Gamma}_i}^H \mathbf{\Gamma}_k = \delta_{i-k}$, the interference term in (33) vanishes, and the P_e reduces to

$$P_{e,ideal} = Q\left(\sqrt{\frac{2M\mathcal{E}}{\sigma^2}\left(\frac{K}{K_{ind}}\right)}\right) = Q\left(\sqrt{\frac{2M\mathcal{E}K_{coh}}{\sigma^2}}\right) \tag{34}$$

which is the P_e for a BPSK signaling system transmitting with K_{coh} times the individual sensor power and the M-fold increase in the received SNR at the WIR is due to array gain. The above formula reveals a basic *rate-versus-reliability tradeoff* mediated by transmission power in AWS at the highest resolution: *increase in rate by increasing K_{ind} (multiplexing gain) comes at the cost of loss in reliability (SNR) due to a decrease in K_{coh}.*

Two extreme cases of this tradeoff are illustrative. On one extreme is the $K_{ind} = 1 \leftrightarrow K_{coh} = K$ case, representing highly redundant/correlated sensing in which all sensors transmit identical bit streams; that is, $\beta_i = \tilde{\beta}_1$ for all i. Since there is no interference, the corresponding error probability is given by

$$P_e = Q\left(\sqrt{\frac{2M\|\boldsymbol{q}_i\|^2\mathcal{E}}{\sigma^2}}\right) \approx Q\left(\sqrt{\frac{2MK\mathcal{E}}{\sigma^2}}\right) \tag{35}$$

since $\|\boldsymbol{q}_i\|^2 = \sum_{i=1}^{K}\sum_{j=1}^{K} {\mathbf{\Gamma}_i}^H \mathbf{\Gamma}_j \approx K$. This case represents the low-rate extreme in which a single bit is retrieved in each channel use, although at K times the per-sensor SNR.

At the other extreme is the $K_{ind} = K \leftrightarrow K_{coh} = 1$ case representing independent sensing where all sensors transmit independent data streams; that is, $\beta_i = \tilde{\beta}_i$ for all i. This case represents high-rate information retrieval and a total of K bits are retrieved by the WIR during each channel use. The probability of error can be expressed as

$$P_e = Q\left(\sqrt{\frac{2M\mathcal{E}\|\mathbf{\Gamma}_i\|^4}{\sigma^2\|\mathbf{\Gamma}_i\|^2 + M\mathcal{E}\sum_{k\neq i}|{\mathbf{\Gamma}_i}^H\mathbf{\Gamma}_k|^2}}\right) . \tag{36}$$

In the ideal case, if the sensor positions are exactly aligned with the center of the angle-delay resolution bins, then there is no interference between sensors and the P_e is given by (34) with $K_{coh} = 1$

$$P_e = Q\left(\sqrt{\frac{2M\mathcal{E}}{\sigma^2}}\right) \tag{37}$$

which is the P_e of BPSK signaling over K parallel AWGN channels each with SNR $M\mathcal{E}/\sigma^2$. In general, the system is interference-limited since the P_e exhibits an error floor in the limit of high transmit SNR

$$P_e \to Q\left(\sqrt{\frac{2\|\mathbf{\Gamma}_i\|^4}{\sum_{k\neq i}|{\mathbf{\Gamma}_i}^H\mathbf{\Gamma}_k|^2}}\right) . \tag{38}$$

Thus, in addition to a loss in received SNR in the ideal case, the high-rate case also suffers from interference in general.

B. Linear MMSE Interference Suppression

As noted above, the P_e based on angle-delay signature matched filtering suffers from an error floor, especially at high values of K_{ind}. Thus, methods for mitigating inter-sensor interference are critical for energy-efficient operation in AWS. The low-power communication channel from the sensor network to the WIR is a multiple access channel (MAC) and the different sensors are analogous to multiple users simultaneously accessing the channel with distinct angle-delay signatures. Thus, a range of multiuser detection techniques [9] can be leveraged. In particular, low-complexity linear interference suppression techniques can yield competitive performance [9]. In this section, we describe a simple linear MMSE interference suppression technique [9], [10].

The basic idea behind MMSE interference suppression is to exploit the differences in the angle-delay signatures for different coherence groups, $\{\boldsymbol{q}_i\}$. This is attained by designing a MMSE filter that jointly operates on all active MF outputs $\boldsymbol{z}$. The filter operates on the MF outputs within each channel use; no joint processing is done across time. Specifically, the detector at the WIR takes the form

$$\hat{\tilde{\boldsymbol{\beta}}} = \mathrm{sign}\left\{\mathrm{Re}\left(\boldsymbol{L}_{mmse}\boldsymbol{z}\right)\right\} \tag{39}$$

where the $K_{ind} \times K$ filter matrix $\boldsymbol{L}_{mmse}$ is given by

$$\boldsymbol{L}_{mmse} = \arg\min_{\boldsymbol{L}} E[\|\boldsymbol{L}\boldsymbol{z} - \tilde{\boldsymbol{\beta}}\|^2] = \boldsymbol{Q}^H\boldsymbol{R}^{-1} \tag{40}$$

where $\boldsymbol{R} = E[\boldsymbol{z}\boldsymbol{z}^H] = M\mathcal{E}\boldsymbol{Q}\boldsymbol{Q}^H + \sigma^2\boldsymbol{I}$ is the correlation matrix of the MF outputs. In (40), $\boldsymbol{R}^{-1}$ suppresses the interference corrupting each of MF outputs and the matrix $\boldsymbol{Q}^H$ performs angle-delay signature matched filtering on the resulting filtered MF outputs. The final decision is then formed as in (39). The i^{th} filtered statistic $\tilde{z}_i$, $i = 1, \cdots, K_{ind}$, can be expressed as

$$\begin{aligned}\tilde{z}_i = \sqrt{M\mathcal{E}}{\boldsymbol{q}_i}^H\boldsymbol{R}^{-1}\boldsymbol{q}_i\tilde{\beta}_i + \sqrt{M\mathcal{E}}\sum_{k\neq i}{\boldsymbol{q}_i}^H\boldsymbol{R}^{-1}\boldsymbol{q}_k\tilde{\beta}_k \\ +{\boldsymbol{q}_i}^H\boldsymbol{R}^{-1}\boldsymbol{w}\end{aligned} \tag{41}$$

where ${\boldsymbol{q}_i}^H\boldsymbol{R}^{-1}\boldsymbol{q}_i$ represents the filtered desired signal and ${\boldsymbol{q}_i}^H\boldsymbol{R}^{-1}\boldsymbol{q}_k$, the suppressed interferers. Using a Gaussian approximation for the interference [9], the P_e for the i-th bit stream can be expressed as

$$P_e(i) = Q\left(\sqrt{\frac{2M\mathcal{E}|{\boldsymbol{q}_i}^H\boldsymbol{R}^{-1}\boldsymbol{q}_i|^2}{\sigma^2\|{\boldsymbol{q}_i}^H\boldsymbol{R}^{-1}\|^2 + M\mathcal{E}\sum\limits_{k\neq i}|{\boldsymbol{q}_i}^H\boldsymbol{R}^{-1}\boldsymbol{q}_k|^2}}\right) \tag{42}$$

We note that the P_e associated with MMSE filtering does not suffer from error floors [9] as confirmed by the numerical results presented in the next section. We note that the computation of the MMSE filter can be done in a variety of ways, in practice [3].

C. Numerical Results

We now illustrate the performance of information retrieval at the highest resolution with numerical results. We consider a WIR equipped with $M = 9$ antennas which transmits a single spread-spectrum waveform in all virtual spatial beams: $s_V(m;t) = c(t)$ for all m, where a length $N = TW = 127$ pseudo-random binary code is used for $c(t)$. We assume that the transmission delays from the sensors to the WIR fall within $L = 12$ delay bins, resulting in a total of $ML = 108$ angle-delay resolution bins at the highest resolution. We also assume that all the bins are "active" with a unique sensor associated with each bin. The sensors transmit their information via BPSK symbols. For simulation purposes, we assume that perfect phase estimates are available at the WIR. In practice, we can estimate the phases $\{\phi_i\}$, as long at they remain constant over two channel uses [3].

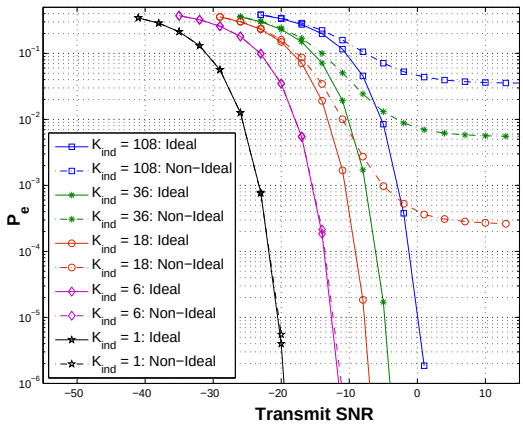

(a)

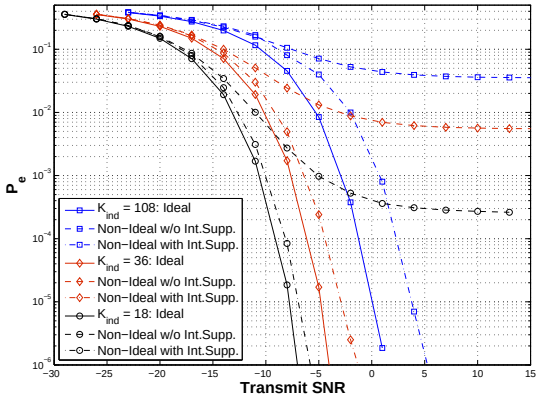

(b)

Fig. 4. P_e vs. SNR plots for an AWS system retrieving K_{ind} bits per channel use at maximum angle-delay resolution. (a) Without interference suppression. (b) With MMSE interference suppression.

The probability of error P_e as a function of the per-sensor transmit SNR, $\rho_{sen} = \mathcal{E}/\sigma^2$, is shown in Fig. 4(a) for different values of K_{ind}. The ideal P_e curves represent benchmarks in which the sensors are located at the center of the bins to eliminate interference. All other P_e (non-ideal) plots correspond to the average performance over multiple random positions of the sensors within their respective bins, and the P_e reflects the average performance across all active sensors. As K_{ind} decreases, the required SNR for a given P_e is reduced due to an increase in K_{coh}. However, non-ideal detection (Fig. 4(a)) incurs a loss in SNR compared to the ideal case and also exhibits a P_e floor due to interference; with increasing K_{ind}, the interference level increases and hence the P_e saturates at a larger value.

Fig. 4(b) illustrates the performance with interference suppression. As evident, AWS with interference suppression delivers remarkable performance and exhibits no error floors in contrast to MF-based detection.

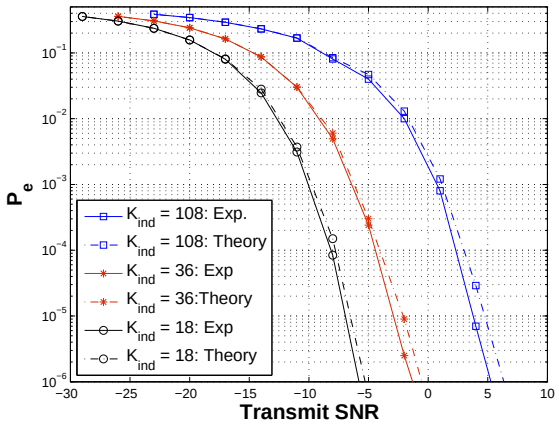

Fig. 5. Comparison of the analytically computed P_e values with numerically estimated values for the non-ideal scenario with MMSE filtering.

Fig. 5 compares the numerically estimated values of P_e (with interference suppression in Fig. 4(b)) with the corresponding analytic expression in (42). The agreement is quite good and the deviations can be attributed to the Gaussian approximation of interference (also noted in [9]).

V. Source-Channel Matching: Information Retrieval Through Angle-Delay Focussing

In information retrieval at maximum resolution each angle-delay resolution bin is associated with a distinct sensor. As a result, each sensor transmission is associated with a distinct MF output, z_i, $i = 1, \cdots, K$, in (27). On the other hand, in the canonical sensing configurations, only $K_{ind} \leq K$ independent bits are transmitted and $K_{coh} = K/K_{ind}$ sensors in each group transmit the same bit. These identical transmissions are coherently combined at the receiver via matched filtering to the effective angle-delay signatures $\boldsymbol{q}_i$, $i = 1, \cdots, K_{ind}$. However, in the process, even in the ideal case, K_{coh} MF outputs, along with their individual noises, contribute to the decoding of the independent bit from each coherence group.

The motivation for matched source-channel communication is to coordinate the transmissions from the K_{coh} sensors in each group so that, in effect, they are *coherently* combined during communication over the channel and the combined

signal gets mapped to a single angle-delay resolution bin at the WIR. Viewed another way, matched source-channel communication converts the $K_{coh} \times K_{coh}$ parallel channels between each coherence group and the WIR into a $K_{coh} \times 1$ coherent multiple access channel (MAC) through a form of distributed *angle-delay focussing*: the K sensor transmissions are now naturally mapped to K_{ind} distinct active angle-delay resolution bins at the WIR (as opposed to K bins at maximum resolution), and K_{coh} sensor transmissions from each group coherently contribute to each active MF output.

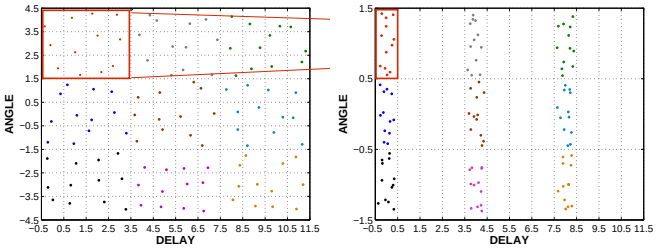

(a) (b)

Fig. 6. Illustration of source-channel matching. (a) Active angle-delay resolution bins at the WIR corresponding to a canonical sensing configuration, $K = K_{ind}K_{coh}$, at the highest resolution; all angle-delay resolution bins are active. (b) Active angle-delay resolution bins at the WIR corresponding to source-channel matching; only K_{ind} angle-delay resolution bins are active at the WIR and K_{coh} sensor transmissions from each group contribute coherently to each bin.

The idea of matched source-channel communication is illustrated in Fig. 6. Let $K_{ind} = M_{ind}L_{ind} \leftrightarrow K_{coh} = M_{coh}L_{coh}$ so that each coherence region with $K_{coh} = 12$ sensors corresponds to $L_{coh} = 4$ delay resolution bins and $M_{coh} = 3$ angle resolution bins at the maximum resolution, as illustrated in Fig. 6(a). Matched source-channel communication involves three key effects in each coherence group, as illustrated in Fig. 6(b): i) the angular resolution is reduced by a factor M_{coh} so that the M_{coh} angle resolution bins in Fig. 6(a) get mapped to a single angle resolution bin in Fig. 6(b); ii) the sensor transmissions in distinct L_{coh} delay resolution bins in Fig. 6(a) are "lined-up" in time so that they lie in a single delay resolution bin as in Fig. 6(b); and iii) the K_{coh} sensors in each group that now lie in a single angle-delay resolution bin in Fig. 6(b) transmit in a phase-coherent fashion.

How do we realize the above three effects in practice to realize a matched source-channel communication network architecture? The first effect can be realized by reducing the antenna spacings at the WIR by a factor of M_{coh} ($M_{coh} = 3$ in Fig. 6) [6]. This effectively results in $M/M_{coh} = M_{ind}$ distinct spatial beams, each with a M_{coh} times wider beamwidth [6]. The second effect can be realized through distributed time-reversal techniques [11] to line up the sensor transmissions in L_{coh} delay resolution bins. The third effect can be realized by applying distributed beamforming algorithms [12] to make the K_{coh} sensor transmissions from each group, that lie in a single angle-delay resolution bin in Fig. 6(b), phase coherent. An alternative approach to realizing the source-channel matching is illustrated in Fig. 7. The lower spatial resolution can be attained by reducing the carrier frequency by a factor of M_{coh}, whereas instead of using time-reversal to align the sensor responses in time, we could alternatively decrease the delay resolution by a factor of L_{coh} by decreasing the signaling bandwidth by a factor of L_{coh}.

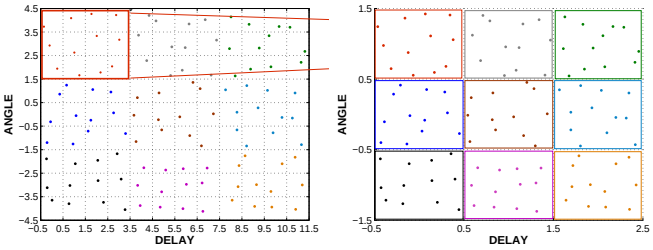

(a) (b)

Fig. 7. Alternative approach to achieving source-channel matching (a) Active angle-delay resolution bins corresponding to a canonical sensing configuration, $K = K_{ind}K_{coh}$, at the highest resolution. (b) K_{ind} active angle-delay resolution bins created via reduced angle-delay resolution.

The effective system equation for matched source-channel communication can be inferred from the system equation (27) at maximum resolution as

$$\begin{aligned} \boldsymbol{z}_{sc} &= [z_{sc,1}, z_{sc,2}, \cdots, z_{sc,K_{ind}}]^T \\ &= \sqrt{M\mathcal{E}}\boldsymbol{Q}^H\boldsymbol{Q}\tilde{\boldsymbol{\beta}} + \boldsymbol{w}_{sc} \\ &= \sqrt{M\mathcal{E}}\sum_{i=1}^{K_{ind}} \tilde{\beta}_i \boldsymbol{v}_i + \boldsymbol{w}_{sc} \end{aligned} \tag{43}$$

where the the $K_{ind} \times K_{ind}$ matrix

$$\boldsymbol{V} = \boldsymbol{Q}^H\boldsymbol{Q} = [\boldsymbol{v}_1, \boldsymbol{v}_2, \cdots, \boldsymbol{v}_{K_{ind}}] \tag{44}$$

represents the effective coupling between the K_{ind} independent bits and the K_{ind} active angle-delay resolution bins at the WIR, and the $K_{ind} \times 1$ vectors, $\boldsymbol{v}_i$, represent the effective angle-delay signatures associated with the i-th independent transmitted bit $\tilde{\beta}_i$. Due to the coherent angle-delay focussing in source-channel matching we have the following relation between $\boldsymbol{v}_i$ and $\boldsymbol{q}_i$

$$\|\boldsymbol{v}_i\|^2 \approx K_{coh}\|\boldsymbol{q}_i\|^2 \approx K_{coh}^2 \tag{45}$$

where the approximations are exact in the ideal case. In the ideal case, the $K \times 1$ high-resolution signature $\boldsymbol{q}_i$ consists of all zeros except K_{coh} ones in the coordinates corresponding to the i-th group of sensors (and corresponding MF outputs). On the other hand, the "focussed" $K_{ind} \times 1$ signature $\boldsymbol{v}_i$ consists of all zeros except a non-zero entry of size K_{coh} in the coordinate corresponding to the i-th group of sensors; the increase in magnitude of the non-zero entry is due to the phase-coherent transmissions from K_{coh} sensors in the group (see Fig. 6(b)).

The receivers at the WIR for matched source-channel communication can be designed using the system equation (43). In particular, the simplest receiver corresponding to angle-delay matched filtering is given by $\tilde{\hat{\boldsymbol{\beta}}} =$

$\text{sign}\left\{\text{Re}\left(\boldsymbol{V}^H\boldsymbol{z}_{sc}\right)\right\}$ and the $P_{e,sc}(i)$ associated with the i-th bit can be estimated via $\text{SINR}(i)$ as in (31) where the expression for $\text{SINR}(i)$ is given by (33) by replacing $\{\boldsymbol{q}_i\}$ with $\{\boldsymbol{v}_i\}$. Similarly, the MMSE receiver is given by $\hat{\tilde{\boldsymbol{\beta}}} = \text{sign}\left\{\text{Re}\left(\boldsymbol{L}_{sc,mmse}\boldsymbol{z}_{sc}\right)\right\}$ where the $K_{ind}\times K_{ind}$ matrix $\boldsymbol{L}_{sc,mmse}$ is given by

$$\boldsymbol{L}_{sc,mmse} = \arg\min_{\boldsymbol{L}} E[\|\boldsymbol{L}\boldsymbol{z}_{sc} - \tilde{\boldsymbol{\beta}}\|^2] = \boldsymbol{V}^H\boldsymbol{R}_{sc}^{-1} \quad (46)$$

where $\boldsymbol{R}_{sc} = E[\boldsymbol{z}_{sc}\boldsymbol{z}_{sc}^H] = M\mathcal{E}\boldsymbol{V}\boldsymbol{V}^H + \sigma^2\boldsymbol{I}$. The P_e of the MMSE receiver can be approximated again using the SINR as in (42)) by replacing $\{\boldsymbol{q}_i\}$ with $\{\boldsymbol{v}_i\}$ and $\boldsymbol{R}$ with $\boldsymbol{R}_{sc}$.

The expression for P_e in the ideal case provides a good reference to compare the performance of matched source-channel communication relative to information retrieval at the highest resolution

$$P_{e,sc,ideal} = Q\left(\sqrt{\frac{2M\mathcal{E}}{\sigma^2}\left(\frac{K}{K_{ind}}\right)^2}\right) = Q\left(\sqrt{\frac{2M\mathcal{E}K_{coh}^2}{\sigma^2}}\right). \quad (47)$$

Comparing the above equation with (34) we note that source-channel matching affords an SNR gain of K_{coh} compared to information retrieval at the highest resolution.

A. Numerical Results

We now present numerical results to illustrate the performance of information retrieval with source-channel matching in AWS. The simulation set up is the same as in Sec. IV-C.

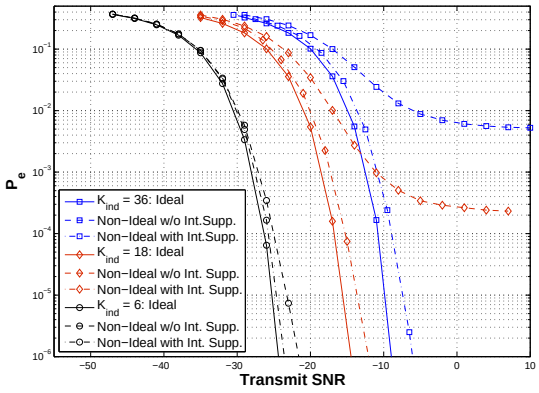

Fig. 8. P_e vs. SNR plots for an AWS sytem using source-channel matching with K_{ind} bits retrieved in each channel use.

The probability of error P_e as a function of the transmit SNR (per sensor) for the source-channel matched configuration is shown in Fig. 8. Note that although the P_e behavior is similar to that of the maximum resolution setup, the SNR required to attain a desired P_e is substantially reduced due to the K_{coh} SNR gain. Non-ideal detection again incurs a loss in SNR and also exhibits a P_e floor due to interference as was the case in Fig. 4. However the performance is near-ideal with interference suppression.

Fig. 9 illustrates the performance gains due to source-channel matching. Even in the practical (non-ideal) scenario,

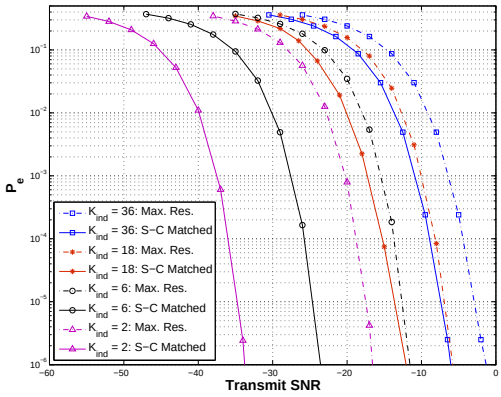

Fig. 9. Comparison of AWS performance at the maximum resolution and that with source-channel matching. Non-Ideal P_e curves with interference suppression.

source channel matching provides a gain of approximately $10\log(K_{coh})$ dB compared to information retrieval at the maximum resolution. For example, when $K_{ind} = 6 \Rightarrow K_{coh} = 18$, the P_e curves are spaced by about 12dB. For a constant K, decreasing K_{ind} increases K_{coh} and hence the gain due to source channel matching is even more pronounced for smaller values of K_{ind}.

VI. Sensing Capacity

Thus far we have analyzed the performance of AWS for uncoded coherent BPSK transmissions from the sensors. In this section, we discusses the notion of sensing capacity in AWS that may be attained via coded transmissions from the sensors. Furthermore, we address the following question: for a given per-sensor SNR, what is the optimal sensing configuration (value of K_{ind}) that maximizes the sensing capacity? As we will see, the answer in the case of source-channel matching is surprising.

For each canonical configuration, K_{ind} parallel channels are established between the sensor ensemble and the WIR. For any given configuration, the sensing capacity can be approximated by using the SINR per parallel channel

$$C\left(K_{ind}\right) \approx \frac{L}{TW}\sum_{i=1}^{K_{ind}}\log_2\left(1+\text{SINR}(i)\right) \text{ bps/Hz} \quad (48)$$

where the factor $L/(TW)$ reflects the fraction of temporal dimensions used for establishing the parallel channels. The above expression can be used for information retrieval at the highest resolution or with source-channel matching as well as with or without interference suppression by plugging in the appropriate expression for $\text{SINR}(i)$.

We are particularly interested in studying the impact of source-channel matching on sensing capacity. Thus, we focus on the ideal case to get insight so that $\text{SINR} \to \text{SNR}$ and its the same for all parallel channels. Furthermore, the capacity expression in this case is exact rather than an approximation and corresponds to the capacity of K_{ind} parallel AWGN

channels, each operating at the same SNR. In the case of information retrieval at the highest resolution we have

$$C_{ideal}\left(K_{ind}\right) = \frac{LK_{ind}}{TW}\log_2\left(1+\frac{M\mathcal{E}}{\sigma^2}\frac{K}{K_{ind}}\right) \qquad (49)$$

whereas in the case of source-channel matching we have

$$C_{sc,ideal}\left(K_{ind}\right) = \frac{LK_{ind}}{TW}\log_2\left(1+\frac{M\mathcal{E}}{\sigma^2}\left(\frac{K}{K_{ind}}\right)^2\right) \qquad (50)$$

which reflects an SNR gain of K_{coh} per parallel channel compared to maximum resolution information retrieval.

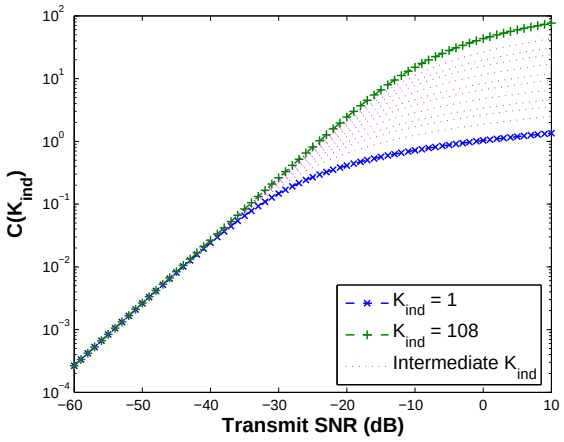

(a)

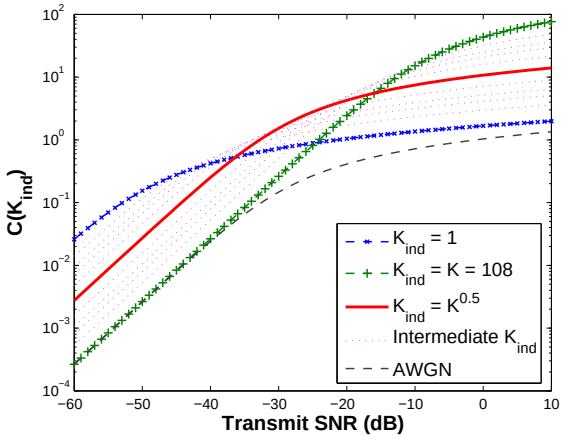

(b)

Fig. 10. Ideal sensing capacity as a function of transmit SNR per sensor for different values of K_{ind}. (a) Information retrieval at maximum resolution. (b) Information retrieval with source-channel matching.

From (49) we note that the ideal sensing capacity is a monotonic function of K_{ind} for information retrieval at the highest resolution. This is illustrated in Fig. 10(a) where the capacity is plotted as a function of transmit SNR per sensor, $\rho_{sensor} = \mathcal{E}/\sigma^2$, for different values of K_{ind}. As evident, at high SNR's, the capacity is maximum for $K_{ind} = K$ and minimum for $K_{ind} = 1$. On the other hand, this increase in capacity with K_{ind} diminishes at low SNR's where the curves for the two extremes coincide.

Fig. 10(b) plots the ideal sensing capacity as a function of ρ_{sen} for source-channel matching for different values of K_{ind}. In this case, the capacity is not a monotonic function of ρ_{sen}. At high SNR's, the $K_{ind} = K$ configuration yields the highest capacity, as before. However, at low SNR's, the $K_{ind} = 1$ configuration yields the highest capacity. Most importantly, at every ρ_{sen} there is an optimum sensing configuration, $K_{opt}(\rho_{sen})$, that yields the highest capacity. In particular, the configuration $K_{ind} = \sqrt{K}$ is a robust choice whose capacity remains between the extreme cases of $K_{ind} = K$ and $K_{ind} = 1$. In fact, the expression for $C_{sc,ideal}$ reveals a fundamental *multiplexing gain versus received SNR tradeoff* that we had also identified recently in the context of MIMO communication over sparse multipath channels [6]: increasing the multiplexing gain (K_{ind}) comes at the cost of decreasing the received SNR per parallel channel, $\rho_{rx} = M\rho_{sen}(K/K_{ind})^2$, and vice versa. The optimal configuration at any ρ_{sen} optimizes this tradeoff to yield the highest capacity. Using the results of [6], we can characterize the optimal configuration, for any operating ρ_{sen}, as

$$K_{sc,opt}(\rho_{sen}) \approx \begin{cases} 1 & , \quad \rho_{sen} \le \rho_{low} = \frac{4}{MK^2} \\ \frac{\sqrt{M\rho_{sen}}K}{2} & , \quad \rho_{sen} \in (\rho_{low}, \rho_{high}) \\ K & , \quad \rho_{sen} \ge \rho_{high} = \frac{4}{M} \end{cases} \qquad (51)$$

Fig. 10(b) also shows the capacity of an equivalent AWGN channel with the total transmit SNR $\rho_{total} = \rho_{sen}MK$ reflecting the situation in which a single sensor (a fusion node) transmits the data using the total power used by the entire network of K nodes. As evident, source-channel matching affords the maximum multiplexing gain over the AWGN capacity over the entire SNR range, reflecting the K-fold distributed MIMO gain in source-channel matching.

REFERENCES

[1] D. Estrin, L. Girod, G. Pottie, and M. Srivastava, "Instrumenting the world with wireless sensor networks," in *Proc. 2001 Intl. Conf. on Acoustics, Speech, and Signal Processing (ICASSP'01)*, May 2001.

[2] *IEEE Journal on Selected Areas in Communications*. Special Issues on Sensor Networks, Aug. 2004 and Apr. 2005.

[3] T. Sivanadyan and A. Sayeed, "Active wireless sensing for rapid information retrieval in sensor networks," in *Proc. 5th Intl. Conf. on Information Processing in Sensor Networks (IPSN'06)*, Apr 2006.

[4] A. Sayeed, "Deconstructing multi-antenna fading channels," *IEEE Trans. Signal Processing*, Oct. 2002.

[5] ——, "A virtual representation for time- and frequency-selective correlated mimo channels," in *Proc. 2003 IEEE Intl. Conf. on Acoustics, Speech, and Signal Processing (ICASSP'03)*, May 2003.

[6] A. Sayeed and V. Raghavan, "The ideal MIMO channel: Maximizing capacity in sparse multipath with reconfigurable antenna arrays," in *Proc. 2006 IEEE Intl. Symp. Inform. Th.(ISIT'06)*, July 2006.

[7] B. Ananthasubramaniam and U. Madhow, "Virtual radar imaging for sensor networks," in *Proc. 3rd Intl. Conf. on Information Processing in Sensor Networks (IPSN'04)*, Apr. 2004.

[8] ——, "Detection and localization of events in imaging sensor nets," in *Proc. 2005 IEEE Intl. Symp. Inform. Th/ (ISIT'05)*, Sept. 2005.

[9] S. Verdu, *Multiuser Detection*. Cambridge University Press, 1998.

[10] S. Haykin, *Adaptive Filter Theory*, 4th ed. Prentice Hall, 2002.

[11] R. J. Barton, J. Chen, and K. Huang, "Cooperative time reversal for communication in power-constrained wireless sensor networks," in *Proc. 43rd Annual Allerton Conference*, Sept. 2005.

[12] R. Mudumbai, J. Hespanha, and U. Madhow, "Scalable feedback control for distributed beamforming in sensor networks," in *Proc. 2005 IEEE Intl. Symp. Inform. Th. (ISIT'05)*, Sept. 2005.